Journal of Fluorescence, Vol. 7, No. 2, 1997

Characterization of a Confocal Microscope for Time-Resolved Photon Counting Fluorescence

Laetitia Schoutteten,[1] Patrick Denjean,[1] and Robert B. Pansu[1,2]

Received July 16, 1996; accepted June 4, 1997

A confocal microscope setup is developed for time-resolved fluorescence measurements. It is added to a traditional cuvette time-resolved setup, with a pumped Ti–Sa light source. The temporal resolution of 37 ps (FWHM) is not degraded, in comparison with the cuvette setup also described. These setups allow both decay lifetime and anisotropy relaxation time determination. Fluorescence correlation spectroscopy (FCS) is used to determine the observation point size. When associated with the calcium probe calcium green, calcium concentration in single cells can be determined in 10 ms by simultaneous acquisition of early and late fluorescence photons.

KEY WORDS: Time-resolved fluorescence; confocal microscopy; anisotropy; fluorescence correlation spectroscopy; calcium probes; laser.

INTRODUCTION

The last 10 years have seen a great development of fluorescent molecules for imagery and measurements of intracellular ions.[1] Calcium has been a prototype ion for this kind of measurements, first because of its importance as a messenger in cellular signaling and, also, because of its selective interaction with BAPTA chelator. After a first generation of probes using fluorescence yield as signal, ratiometric probes, like Fura-2, have been developed. The fluorescence intensity ratio recorded for two excitation wavelengths gives an estimation of the calcium concentration which is independent of the probe loading in the cell. A third generation of probes is now proposed, where the free and the bound forms of the probe differ by their fluorescence lifetimes. We show that time-based probing[2] leads to acquisition time limited only by photon flux.

In many cases, lifetimes are more sensitive to the environment than fluorescence or absorption spectra. Thus, careful measurement of decay profiles can be a way to take into account other problems encountered in intracellular probing, such as the adsorption of the probe on proteins,[3] incomplete hydrolysis of precursors,[4] or probe compartmentalization.

Phase fluorimetry was proved to be the most elegant way to obtain time-resolved fluorescence pictures. There are fields where photon counting can be more efficient. In microscopy, bleaching of the sample reduces the acquisition time and only single-photon counting takes advantage of each single photon. Time-resolved photon counting is less sensitive to sample bleaching, as all "frequencies" are simultaneously acquired. It allows us simultaneously to estimate lifetime evolution in a few milliseconds and to construct fluorescent decay curves over minutes, which permits us to validate the hypothesis about probe properties.

[1] ENS Cachan, PPSM (Photophysique et Photochimie Supramoléculaires et Macromoléculaires), URA 1906 CNRS, 61 avenue du Président Wilson, 94235 Cachan Cedex, France.

[2] To whom correspondence should be addressed.

1053-0509/97/0600-0155$12.50/0

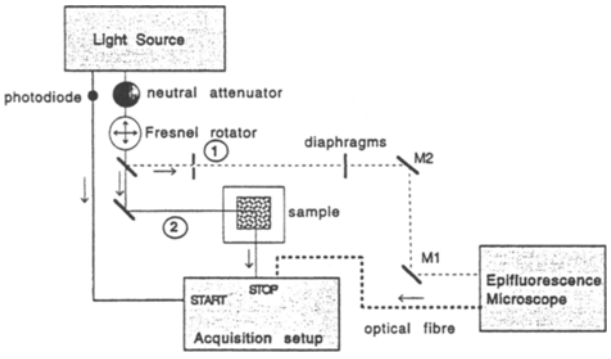

Fig. 1. Time-correlated single-photon counting setup. The light source is a titane-doped sapphire laser, pumped by an argon ion laser delivering 1.2-ps FWHM pulses. Various wavelengths are obtained by using doubling and tripling crystals. Different optical accessories are used: a Fresnel rotator to choose the polarization, a neutral density filter to reduce the beam power, and diaphragms to align the laser beam. The laser beam excites the sample, under the microscope (1) or in the cuvette (2). For the microscope setup, the beam is introduced through the epifluorescence pathway. The fluorescence light is collected through an optical quartz fiber, positioned on the video exit of the microscope. For both setups, the first photon of fluorescence releases the "start" signal of the TAC; the "stop" is provided by the photodiode. The signal is studied with the TMCA acquisition card, which creates the decay curves. The direct fluorescence intensity can also be recorded.

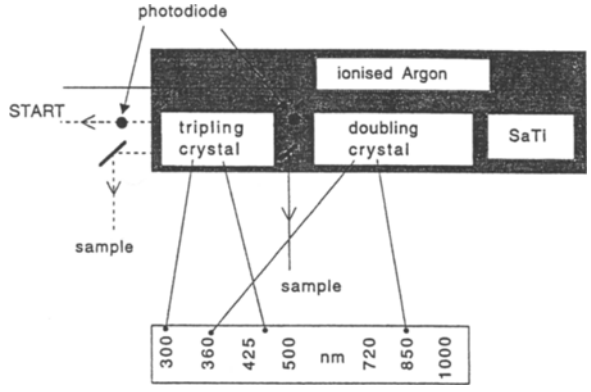

Fig. 2. Doubling and tripling crystals are used to obtain a wide range of wavelengths, from 290 to 1000 nm.

MATERIAL

Setup

Light Source

Decay curves are collected with a time-correlated single-photon counting setup[5] (Fig. 1). The light source is a titane-doped sapphire laser (Spectra Physics, Tsunami 3950B), pumped by an argon ion laser (Beam Lock 2080-12, Spectra Physics) delivering 1.2-ps FWHM pulses (as measured by Galaup[6] using optical autocorrelation), with a repetition rate of 82 MHz.

A pulse selector (frequency doubler and selector, Model 3980, Spectra Physics) reduces the repetition rate to 4 Mhz. This allows complete sample recovery between two excitations.

We use two doubling crystals (Fig. 2), one from Spectra Physics, which is optimized to operate between 360 and 430 nm, and one from GWU, operating from 420 to 498 nm. The second doubling crystal (LBO; lithium β-borate oxide) is followed by a tripling one which permits excitation from 290 to 305 nm.

Change in the operating wavelength of the Ti–Sa laser induces a translation of the laser beam after the doubling crystal, for the GWU doubling device, but this is corrected with the Spectra Physics one.

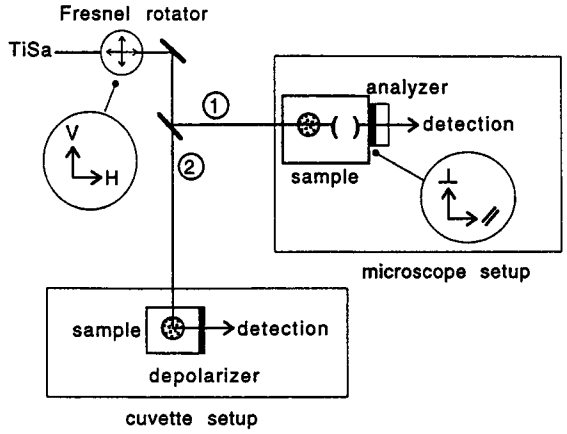

Fig. 3. This setup allows polarization measurements for each configuration, in the cuvette or under the microscope. The laser beam polarization, initially linear, can be turned using a Fresnel rotator. For the microscope setup (1), an analyzer is used, so that the perpendicular or parallel component of the fluorescence is measured. For the cuvette setup (2), a depolarizer is added in front of the monochromator.

Light Polarization

The laser beam is linearly polarized. The polarization can be turned vertically or horizontally with a Fresnel rotator (Figs. 1 and 3). Real incident laser beam polarization is checked for both setups using a polarizer.

For anisotropy measurement in the microscope setup, an analyzer is placed in front of the fiber to measure the perpendicular or parallel component of the fluorescence. The light is assumed to be totally depolarized when traveling through the optical fiber when it reaches the monochromator. For anisotropy measurements in the

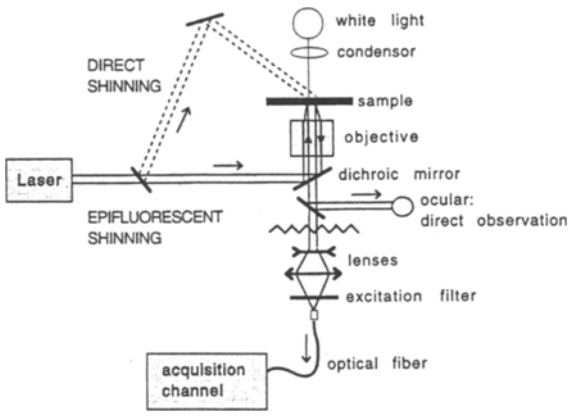

Fig. 4a. In the epifluorescence pathway, the laser beam is sent through the dichroic mirror. The objective convergence is used so that the beam is focused on the sample. Fluorescence is then sent back to the dichroic mirror, which is chosen to be transparent at this wavelength, then reaches the optical fiber entrance, pluged at the microscope video exit. Optics are added so that the beam focuses in the fiber pinhole. The fluorescence signal is sent to the photocounting acquisition channel. Another part of the fluorescence is sent to the ocular for direct observation.

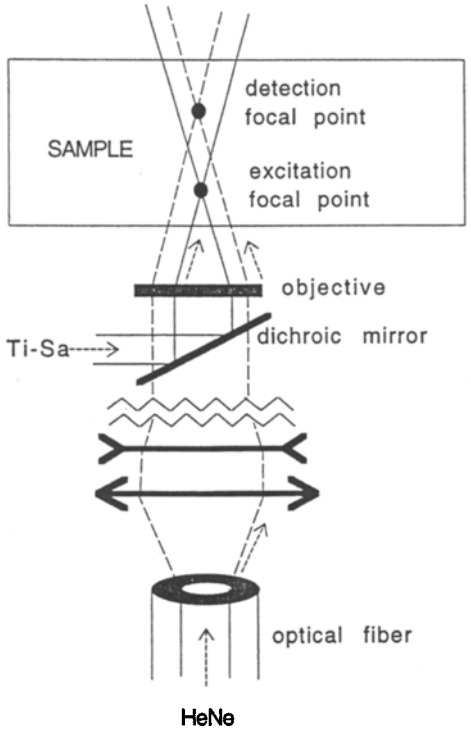

Fig. 4b. Two mirrors are used in the laser beam pathway to overlay the beam on the objective optical axis. The bright focal point must be vertical and brought to the center of the ocular target. To make the microscope confocal, we use a He–Ne laser, which is injected in the detection optical fiber. Both spots are overlaid, which means that observation and excitation spots are confused.

Table I. Nikon Objectives (NA = Numerical Aperture)

Ref.	Magnification	NA
133218	20	0.4
134246	40	0.55
Fluor 100	100	1.3 (oil)
Ph2 20 DL	20	0.4
Ph1 10 DL	10	0.25

cuvette, a depolarizer is added in front of the monochromator.

The beam power can be reduced with a variable neutral density filter with an optical density from 0 to 3.

Light Path

The laser beam is roughly aligned thanks to two diaphragms which allow quick and easy alignments of the beam. The laser beam excites the sample, under the microscope or in the cuvette (way 1 or 2, Fig. 3).

For studies under the microscope[7] (Fig. 4a), the beam is introduced through the epifluorescence pathway. We use an inverted microscope for epifluorescence (NIKON Diaphot 200).

Natural divergence of the laser beam, smaller than the back aperture of the objectives, does not induce supplementary loss.

Two mirrors are used to overlay the laser beam on the objective optical axis (Table I). The closest mirror M1, which influences mainly the beam direction, is used to bring the bright focal point to the center of the objective target, seen through the ocular. The other mirror M2 is adjusted so that the beam emerging from the sample is vertical as visualized by a thick fluorescein block. Another way to check correct alignment is to defocus the objective: the spot should widen, without any distortion.

The fluorescence light is collected through an optical quartz fiber [Oriel; SFS400/440N; 400-μm core diameter; numerical aperture (NA), 0.4 or CM28G62; 62.5-μm core diameter; NA 0.2], positioned on the microscope video exit. The fluorescence image is focused on the fiber entrance with a lens. The fiber entrance can move in the x, y plane with a submillimeter microcontrol system.

Superposition of excitation and detection spots is critical and essential for efficient collection of fluorescence light. For the coarse overlay of the observation and excitation spots, a helium neon laser is injected in the optical fiber (Fig. 4b). Both spots have to be overlaid

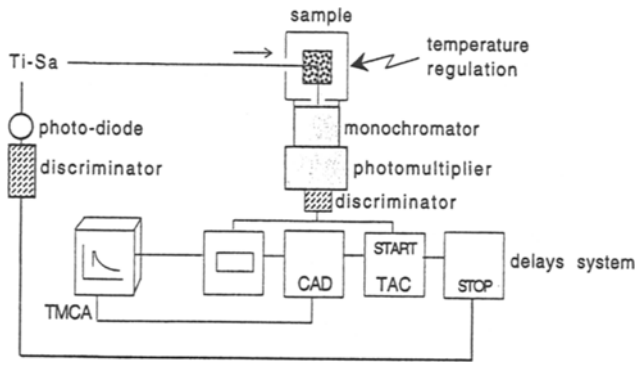

Fig. 5. The fluorescence signal is sent to the acquisition channel. In the microscope setup, the signal is collected via the optical fiber. In the cuvette setup, the right angle configuration limits the diffusion. This apparatus includes the usual constituents: monochromator, photomultiplier, discriminator, and time amplitude converter (TAC). The configuration for the single-photon counting acquisition is original: the "start" signal of the TAC is released by the first photon of fluorescence, and the "stop" signal is provided by the photodiode, positioned after the light source. The signal is computed by the TMCA card, under the PC, which creates the decay curves. Early and late photons can also be independently counted, which ratio is used for the [Ca] determination.

with the reticule center. This confocal arrangement allows the highest resolution in far-field optics.

The objectives (Table I) are movable with a 10-μm step. The objective, with a magnification of 100, is an immersion one. The sample can be moved in the horizontal plane.

Detection

Fluorescence light is collected through two quartz lenses for the cuvette setup. The configuration is a right-angle one (Fig. 5). In the microscope setup, the image from the fiber exit, which collects the fluorescence, is focused in the monochromator entrance slit.

The detection wavelength is selected by a monochromator (Jobin Yvon H10) and detected by a photomultiplier (PM; Hamamatsu Multi Channel Plate R3809U). A constant fraction discriminator (Institut de Physique Nucléaire d'Orsay, France) is positioned directly behind the PM. It has been optimised for PM signal detection with a triggering threshold of 3 mV. This avoids the use of a preamplifier and improves the jitter. In addition, it can be put just behind the PM. This completely suppresses electromagnetic interferences. The time amplitude converter (TAC) was purchased from Tennelec (TC864). The first fluorescence photon releases the "start" signal of the TAC. The "stop" signal, provided by the photodiode positioned after the doubling crystal, on the original beam that was been doubled in frequency, is delayed in a BNC cable of 25 m, in order to arrive after the fluorescence photon on the TAC.

A single fluorescence photon gives the "start" signal, and the photodiode the "stop." This configuration prevents the TAC from launching on each laser pulse, whether there is fluorescence or not. The counting rate is thus improved.

The TAC produces a pulse whose amplitude (between 0 and 10 V) is proportional to the delay between the "start" and the "stop." This amplitude is numerized by an analog digital converter (ADC). This arrangement allows measurements of very short duration, about 2 ps, compared to usual timers, with 100-ps timing resolution. But both the TAC and the ADC have a limit of count rates of 10,000 counts per second, as they need a resetting and processing time of about 2 μs.

The signal is studied via a PC with the TMCA multichannel analyzer card, which creates the decay curves. The numerized value of the delay is used to increment a memory in the multichannel analyzer, which creates histogram of the number of photons of a given delay τ: this is the fluorescence intensity decay. As other photon counting techniques, the signal has a good characterized signal-to-noise ratio.

The expected number of counts in the channel τ is the sum of independent random trials of probability $\exp(-k\tau)$, assuming an exponential decay of rate k. Thus it has a Poisson distribution of mean $\exp(-k\tau)$, with a standard deviation that can be estimated by the square root of the number of counted photons $\sqrt{N}$. Neighbor channels counts result from independent measurements and, to a large extent, are not correlated.[8]

Time-resolved single-photon counting, like phase fluorimetry, is a phase-lock detection. Indeed, an impulsion that arrives at time t can be counted on channel τ if the TAC has been started at time $t - \tau$, so that, after accumulation on t,

$$I(t) = \int_{-\infty}^{+\infty} L(t - \tau)[\exp(-k\tau) + \text{noise}(\tau)]dt$$

where $L(t - \tau)$ is the laser light pulse train.

$$I(\tau) = \int_{-\infty}^{+\infty} L(t - \tau)\exp(-k\tau)dt + \int_{-\infty}^{+\infty} L(t - \tau)\text{noise}(t)dt$$

where the first term is the convoluted fluorescence decay and the second the frequency filtered noise. Thus asynchronous noises contribute to the dark current, whereas only synchronous noises contribute to the signal.

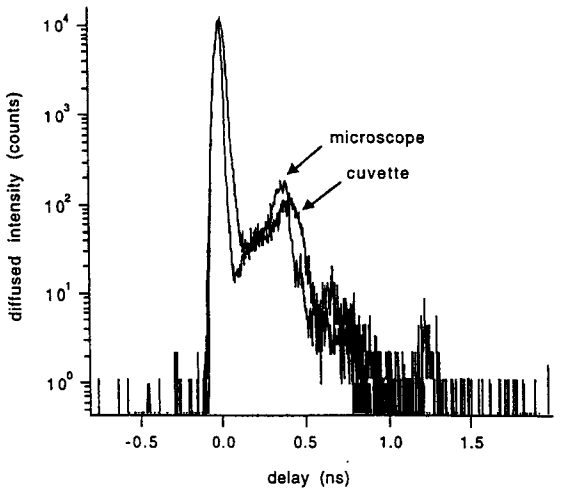

Fig. 6. Pulses at 445 nm, on a TiO_2 solution, recorded in the cuvette setup or under the microscope; 400-μm-diameter optical fiber. We achieved 37 ps in the microscope.

Lifetime Probing

By adding two single-channel analyzers at the TAC exit, we can get two counting channels for the early and late photons. This allows simultaneous acquisition of these two intensities, whose ratio is used to measure the calcium concentration, with the calcium green probe. This probe is characterized by different fluorescence lifetimes when it is complexed with calcium or not. The contribution of the long lifetime is all the more important with an increase in the calcium concentration.

The thresholds of both single-channel analyzers are adjusted so that the same number of photons is counted in the two ways. Then the signal-to-noise ratio is improved and the calcium concentration calculation is more accurate. With a maximal counting rate of 20,000 counts for the TAC, we get 10,000 counts per second in each channel. The count statistic in each ways has a Poisson distribution. A measurement of the ratio with a precision of 20% requires 200 photons to be counted in each channel, which means a measurement time of 10 ms per point. In many cases, the counting rate is not limited by the electronics performance but by the photon flux from the sample.

Data Analysis

The data are exported from PC to Mac to be analyzed with Igor 3.0 (Wavemetrics), which decomposes decays curves as multiexponentials. Mathematica and Matlab are used to find and perform decomposition as a linear combination of reference decays. This decomposition is used for $[Ca^{2+}]$ determination.

SETUP PERFORMANCES

Time Resolution

In single-photon counting, the decay curve is the convolution product of the instrumental response function of the detection by the real decay. The instrumental response function (IRF) is characterized by its full width at half-maximum (FWHM). The IRF is measured from the light scattered by a TiO_2 solution, in the cuvette or under the microscope. Scattered light is measured by recording the diffused intensity of the sample, without any excitation filters.

The IRF is limited by the fluctuation in the duration of the electron avalanche in the multichannel plate.

We achieve 37 ps in the cuvette and in the microscope setup and measure routine values of 50 ps (Fig. 6).

Pulses recorded under the microscope, whatever the fiber is, have a similar FWHM to those recorded for the cuvette setup. The discriminator threshold can be fixed at 15 mV to get the best FWHM. The pulses are shown to be thinner as the threshold is higher, as predicted. A high threshold prevents noise from being detected but significantly reduces the detected fluorescence signal. The value of 4.5 mV is found to be particular for this setup because the signal increases dramatically. We can suppose that the detection setup is counting its self-noise.

For most fluorescent probes (in particular, for calcium green) lifetimes are greater than 0.5 ns so a deconvolution procedure is not required.

Finally, no back-scattered light has been seen from our Nikon objectives (Table I). The 400-μm fiber, low-intensity (whichever the way of reduction, diaphragm or neutral attenuator), microscope setup allows a better instrumental response function of the detection.

Spatial Resolution

Depth of Field

The depth of field is determined by studying the diffused intensity of a 0.1-μm latex sphere film versus the vertical displacement of the different objectives which are used. It is all the smaller as the magnification is important (Fig. 7a) as predicted.[9a,b]

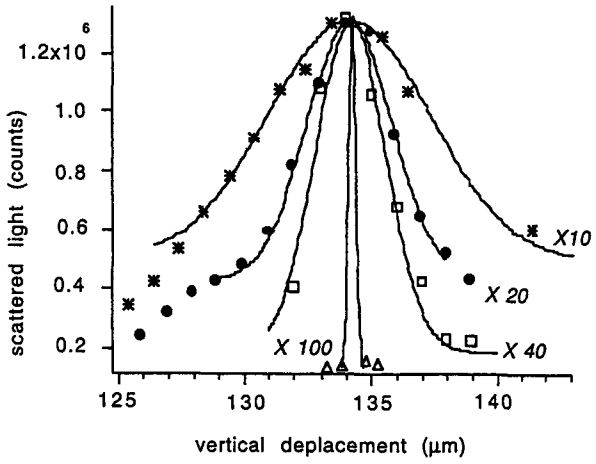

Fig. 7a. Sample: 0.1-µm latex sphere solution. λ excitation = λ emission = 380 nm. The depth of field is determined by recording the scattered light of a thin film, using different objectives (×10, ×20, ×40, ×100—oil). The width of the gaussian fit is shown to be all the more small as the magnification is important, as predicted.

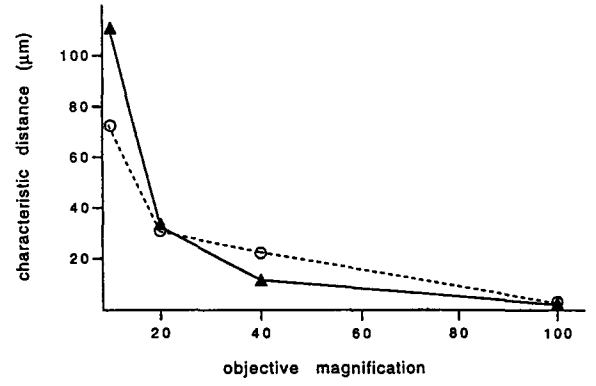

Fig. 7b. Characteristic distance of the microscope objective vs the objective magnification. The optical fiber is 400 µm in diameter; λ excitation = 450 nm, for objectives 10, 20, 40, and 100. The full width at half-maximum (FWHM) of the gaussian fit (○) can be compared to the characteristic distance (▲) calculated from Ref. 9.

The depth of field can be defined as the characteristic distance at which the collected intensity is one-half of that collected in focus. This combines the effect of deposed intensity and collection efficiency. In a semi-geometric approximation, the depth of field Z is given by[9b]

$$Z = \frac{\cos^2(u/2)^* S_0}{\sqrt{1 - \cos^4(u/2)}}$$

where S_0 is the radius of the field diaphragm, that is, the size of the pinhole divided by the magnification; u is the half cone angle defined by the objective lens; and n is the refraction index medium in which the lens is immersed. The numerical aperture is given by

$$NA = n\sin(u)$$

Experimental values and Z are compared in Fig. 7b.

Observation Volume and Waist

The size of the observation point is determined by fluorescence correlation spectroscopy (FCS).[10–13] This method allows the measurement of the focal point size from the kinetics of the fluctuations of fluorescence intensity. Indeed when only a few molecules are present in the observation volume, their number fluctuates around the average value. The relative amplitude of those fluctuations is a measure of the number of molecules that gives, for a known concentration, the observation volume. These fluctuations have a characteristic duration which is the diffusion time of the particle through the observation volume. This time depends on the particle size and observation volume.

Assuming a Brownian motion of particles, the amplitude of concentration fluctuations and their average duration can be determined, from the intensity data, by calculation of the autocorrelation function of the fluorescence intensity $G(\tau)$. $G(\tau)$ gives an estimate of the resemblance between the intensity of fluorescence at time t and $t + \tau$.

$$G(\tau) = \lim_{T \to \infty} \frac{1}{T} \int_0^T \frac{i(t+\tau)i(t)}{\langle i \rangle^2} dt$$

By fitting Eq. (1) to the data, we can determine the dimensions of the excited volume, at focal point Z for vertical direction (the depth of field) and ω in the sample plane (the waist).

$$G(\tau) - 1 = \left(\lim_{T \to \infty} \frac{1}{T} \int_0^T \frac{i(t+\tau)i(t)}{\langle i \rangle^2} dt\right) - 1 = \frac{1}{N}\left(\frac{1}{1 + 4D\tau/\omega^2}\right)\left(\frac{1}{1 + 4D\tau/Z_e^2}\right)^{1/2} \quad (1)$$

where D is the diffusion coefficient of the fluorescent particle, given by the Stocks Einstein relation $D = kT/6\eta R$; R, the particle radius; η, the solvent viscosity; and $i(t)$, the measured fluorescence intensity at time t.

We have recorded the autocorrelation function of the fluorescence intensity fluctuation for the 100× objective.

The sample is a suspension of fluorescent latex particles of 1-µm diameter (Crimson, Molecular Probes). By dilution, concentrations are obtained from 2 to 0.02%, by weight. As required,[10] the z axis is defined by the propagation axis and the sample cell dimensions in the x, y directions are larger than the beam diameter.

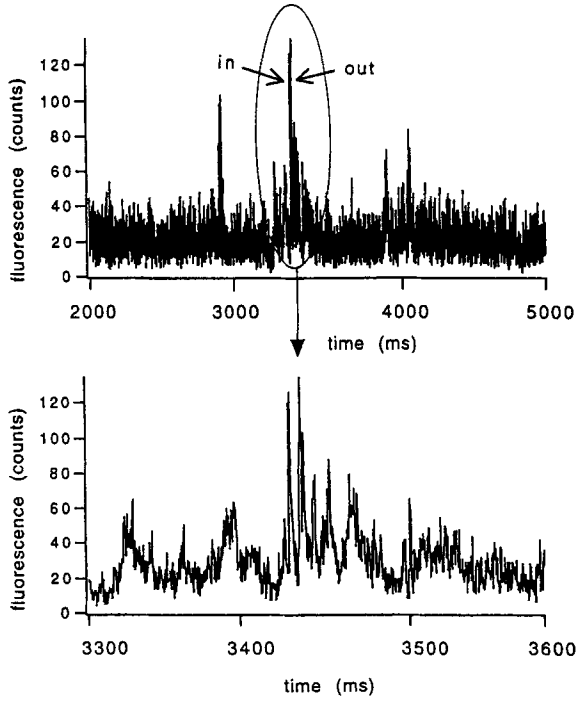

Fig. 8a. By studying the fluorescence intensity recorded from a latex sphere droplet, we can determine the laser beam dimensions. Entrance (*in*) and exit (*out*) of the particule in the spot are observed.

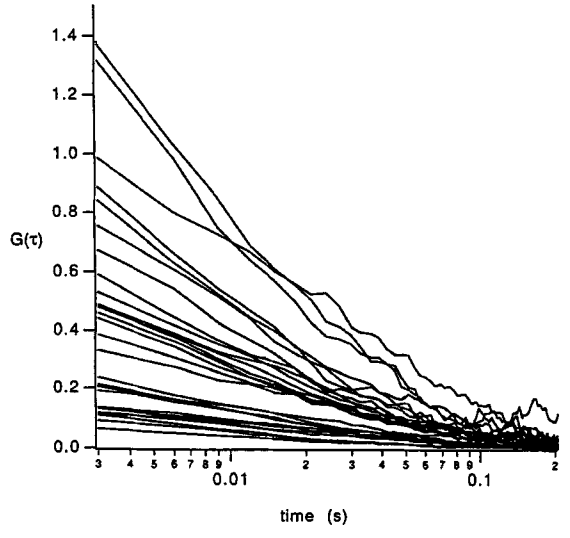

Fig. 8b. This family of autocorrelation curves is obtained on a set of latex suspensions (0.1-μm diameter) fitted by Eq. (1). The reciprocal of the time 0 amplitude equals the number of latex particles in the sample volume at focal point.

We studied a solution droplet between two coverslip glasses to prevent evaporation (0.5 × 0.5 × 1-mm dimensions). The sample is exited by a continuous-wave He–Ne laser.

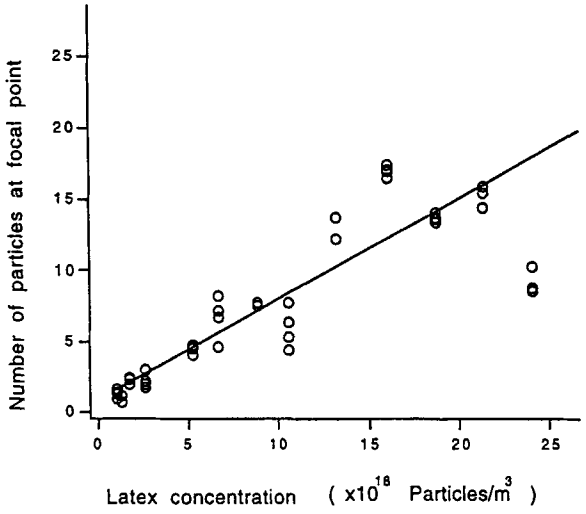

Fig. 8c. The reciprocal of the time 0 autocorrelation curve is plotted versus the sample concentration. The noise observed for the high concentrations is due to the low amplitude of the concentration fluctua-

We get the typical signal shown in Fig. 8a. When the particle crosses the excitation spot, a fluorescence flash appears: we can see the entrance and the exit of the particle in the observation point.

Autocorrelation curves (Fig. 8b) are fitted according to Eq. (1). The reciprocal of their amplitude is plotted versus the latex concentration (Fig. 8c). From the slope, we deduce an observation volume of 7.27 10^{-19} m^3. In Fig. 8 is reported the observation radius with a value of 0.4 μm.

Acquisition Rate and Depth

Detection of rare and short events requires a high acquisition rate and a large memory. Acquisition rate is limited by the TAC and ADC converter to 30,000 counts/s. For detection of short events, we collect at 3-ms time intervals with a storage depth of 16,000 memories, which corresponds to a 48-s observation duration. This allows us to obtain a detailed intensity profile of rare events (Fig. 8a).

Acquisition Duration

We note that decay curves are the same, whatever the apparatus is, in the cuvette or under the microscope. Decays obtained under the microscope must be recorded longer because the sample thickness is smaller than in the 1-cm cuvette. For biological applications (that is, the intracellular calcium concentration determination), we have to find a compromise between a powerful laser

Table II. m s, Saccharose Mass for 100 ml of Pure Water (g); v, Solution Viscosity (cp)[a]

Sample	m s	v
0	0	1
1	5	1.013
2	193	1.66
3	338.1	2.357
4	443.2	3.156
5	584.9	4.9353
6	707.4	7.51
7	943.1	13.26
8	1015.7	20.31

[a]Viscosity is determined from the percentage mass of the saccharose [22].

beam, which destroys the cell but allows a quick and intense response, and a low-power laser beam, which permits long acquisitions by handling the cells carefully but produces a bad signal-to-noise ratio.

Anisotropy Measurements

As described previously, a Fresnel rotator is placed just after the laser (Fig. 1) to choose the polarization of the incident light on the sample, horizontal or vertical (Fig. 3). Intrinsic anisotropy, which is measured at time 0, gives information about the probe spectroscopy and amplitude of ultrafast libration.[15] In a microscope, the conic nature of the excitation and detection beams reduces the anisotropy amplitude by a factor that depends on the objective numerical aperture and on the coverage of the back aperture.[16]

The absolute anisotropy contains little information about the microscopic sample. The fluorescence anisotropy relaxation time gives information about the probe rotational diffusion,[17] probe volume and solvatation,[18] local viscosity[19] or adsorption on protein,[20] and aggregation state.[12]

The characteristic rotational time ϕ is given by the monoexponential curve fit of the anisotropy decay curve $a(t)$.

Neglecting convolution by the instrumental response function, anisotropy is given by

$$a(t) = \frac{I_{\parallel}(t) - I_{\perp}(t)}{I_{\parallel}(t) + 2I_{\perp}(t)} \qquad (2)$$

$I_{\parallel}(t)$ is the decay curve obtained for a polarization parallel to the excitating electric field, and $I_{\perp}(t)$ the decay curve obtained for a polarization perpendicular to the excitating electric field.

In a classical spectrofluorimetric device, excitation and detection beams are perpendicular. Polarization of the excitation beam is vertical. Thus $I_{\parallel} = I_{vv}$ and $I_{\perp} = I_{vh}$, where the subscript stand for the direction of the analyzer. Due to the monochromator dichroism, I_{vh} is further corrected by a $\beta(v)$ factor. In an epifluorescence microscope setup, excitation and detection beams are parallel.

To valid both setups, we have compared anisotropy decay curves and anisotropy relaxation times to those obtained by state fluorimetry fluorescein reference results published previously.[21] The viscosity of the aqueous fluorescein salt solution was varied by the addition of saccharose (Table II). Each decay is counted with a maximum value approximately equal to 10,000 to have a good signal-to-noise ratio. The curves are then normalized to the same value at long times (>3 ns), where fluorescence relaxation no longer depends on polarization, which interacts mainly in the first part of the decay curve (0–3 ns).

Decay curves obtained in the cuvette or under the microscope, and fluorescence spectra are recorded with the same solutions during the same day to prevent solution transformation and result distortion.

Anisotropy decays curves are all the slower since the saccharose concentration is high, because the molecule rotation is hindered by the environment (Fig. 9a).

In the Microscope Setup

In the microscope setup, light polarization (incident/emitted) is rotated because the beam is reflected twice (dichroic mirror and lateral video port). Thus a vertical excitation associated with a horizontal detection I_{vh} corresponds to $I_{\parallel}$ and $I_{vv} = I_{\perp}$. Decay curves (Fig. 9b) have a typical shape, where the $\perp$ and $\parallel$ components are clearly identifiable. A supplementary decay curve is performed, without any analyzer before the optical fiber, D_0, so that the total fluorescence is measured. This D_0 curve is decomposed as a linear combination of the two other decays, $D_{\perp}$ and $D_{\parallel}$ (horizontal and vertical). The influence of each component, for the eight concentrations of saccharose we used (Table II), is shown to be the same. This setup does not add any supplementary parasite polarization of fluorescence light: each component is transmitted with the same efficiency (Fig. 10).

Anisotropy curves (Fig. 11) are fitted with an exponential function,

$$a(t) = a_0 e(-t/\phi)$$

which gives the rotational time ϕ. Parameters are recovered using the least-squares iterative procedure, with the Levenberg–Marquardt algorithm from Igor. Fit validity

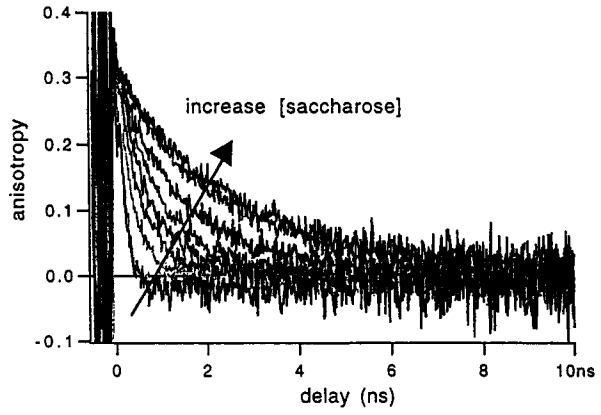

Fig. 9a. The relaxation characteristic time, obtained from anisotropy curves, increases with the saccharose concentration, as predicted.

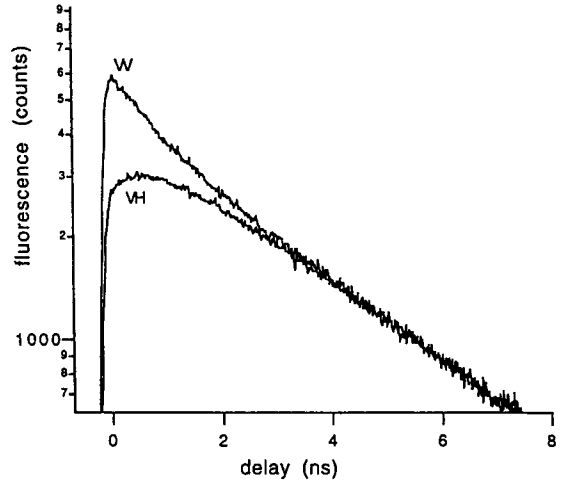

Fig. 9b. The decay curves obtained for both detections, perpendicular and parallel to the incident one (VV, VH), have typical shapes.

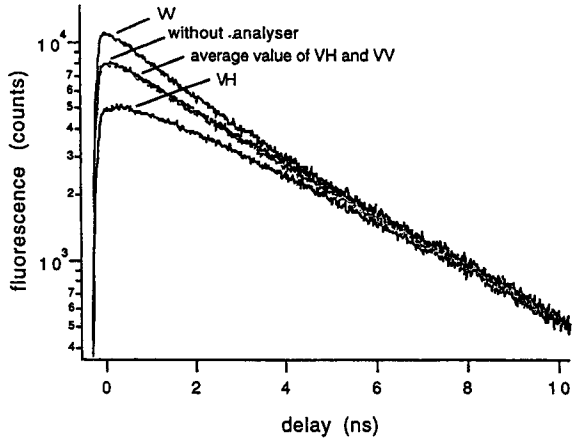

Fig. 10. By measuring the decay without a polarizer, we obtain a profile which has the same contribution of both decays, VV and VH. This has been measured for all saccharose concentrations. Our setup does not add supplementary polarization.

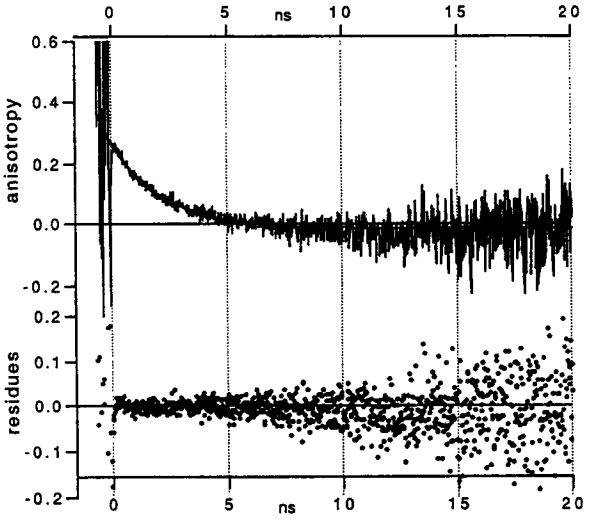

Fig. 11. Anisotropy decay is fitted with an exponential curve, whose characteristic time gives the inverse of the rotational time, ϕ. The validity of this fit is checked with the good zero average value of the residuals.

Table III. Direction, in Degree, of Polarizer and Analyzer, for the Fluorescence Intensity Subscript

	Polarizer	Analyzer
vv	90	90
vh	90	0
hh	0	0
hv	0	90

is checked by the good residues. The average value of $a_0 = 0.337 \pm 0.024$ ($\lambda_{exc} = 437$ nm) is in good agreement with the 0.344 value.[21]

In the Cuvette Setup

For the cuvette setup, polarization is also chosen with the Fresnel rotator (vertical or horizontal), and the total fluorescence is recorded with a depolarizer placed before the monochromator.

Because of the presence of the depolarizer, I_v and I_h turn to

$$I_v(t) = I_{//}(t) + I_{\perp}(t)$$
$$I_h(t) = 2I_{\perp}(t)$$

This is in agreement with the decay curve form.

Finally, anisotropy, defined in Eq. (1), becomes

$$a(t) = \frac{I_v(t) - I_h(t)}{I_v(t) + \mu/2I_h(t)} \qquad (2^*)$$

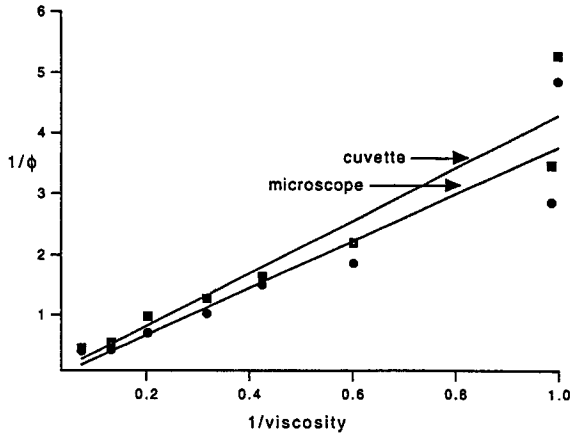

Fig. 12. From the plot of the inverse of the rotational time ($1/\phi$) vs the inverse of the solution viscosity (1/viscosity), we can determine a_0 = 0.36, from the interpolated value for $\eta = 0$.

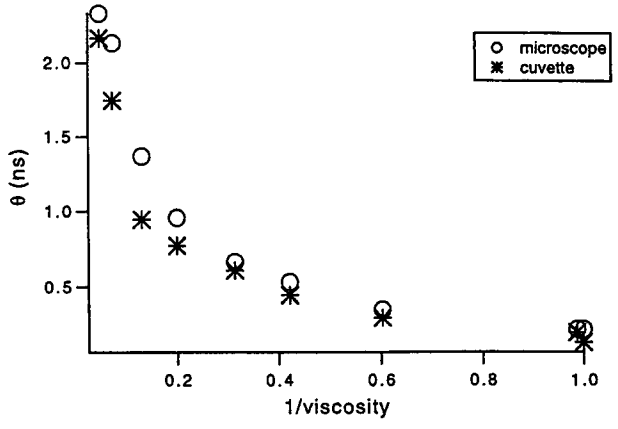

Fig. 13. The rotational relaxation time ϕ is the same whatever the apparatus is, microscope or cuvette. The solutions are saccharose + fluorescein + water, of various viscosities.

To prevent the results from being damaged by excitation light variations, which are supposed to be linear, four acquisitions are performed for each measurement, following the sequence vertical/horizontal/horizontal/vertical [$I_{v1}(t)$, $I_{h1}(t)$, and $I_{h2}(t)$, $I_{v2}(t)$]. To improve the signal-to-noise ratio, as previously in the microscope setup, 10,000 counts are collected in the peak channel and then long time decay parts are stacked.

Finally, the anisotropy is

$$a(t) = \frac{I_{v1}(t) + I_{v2}(t) - I_{h1}(t) - I_{h2}(t)}{I_{v2}(t) + I_{v2}(t) + \mu/2\left[I_{h1}(t) + I_{h2}(t)\right]}$$

with $I_v(t)$ and $I_h(t)$ the decays obtained for each conformation. Anisotropy, fitted by a monoexponential curve, gives an average value of $a_0 = 0.329 \pm 0.024$.

Finally, the results obtained with both setups are comparable (Fig. 13).

Fluorescence Spectrum

Anisotropy curves recorded in both setups are comparable. These results have to be compared with the a_0 value, obtained from fluorescence spectrum with the same solutions. These one are recorded with a SPEX (Jobin Yvon, France): slides, 1.25 mm; HV, 800 V. Anisotropy is given by

$$a = \frac{I_{vv} - I_{vh}}{I_{vv} + 2I_{vh}}$$

Each measurement must be corrected:

$$i_{vv}(\lambda) = I_{vv}g_v$$
$$i_{vh}(\lambda) = I_{vh}g_h$$

where i_{vv} and i_{vh} are the measured values and I_{vv} and I_{vh} are the real values.

Correcting factor g is given by $g = I_{hv}/I_{hh}$.

Finally,

$$a = \frac{I_{vv} - gI_{vh}}{I_{vv} + 2gI_{vh}}$$

The reciprocal of the average value of a (Fig. 12) can be plotted versus the reciprocal of the viscosity 1/2. Interpolated value of a for $\mu/2 = 0$ gives $a_0 = 0.36 \pm 0.031$, which is in agreement with Ref. 21.

Measurements on Living Cells

Living pancreatic cells have been studied under the microscope, marked with the calcium-dependant probe, calcium green, purchased from Molecular Probes. Fluorescence decay profiles are correlated with calcium activity.

We can study one cell at a time (Fig. 14). We have systematically observed a broad distribution of calcium levels in different cells. This was true for native cells as well as for cells whose calcium level was fixed by the use of calcium buffer and ion carrier.

CONCLUSION

Time-resolved single-photon counting can be performed under the microscope. Confocal lighting is achieved simply by introducing a parallel laser beam on the optical axis of the epiillumination setup. Time resolution of the counting chain is not deteriorated by the

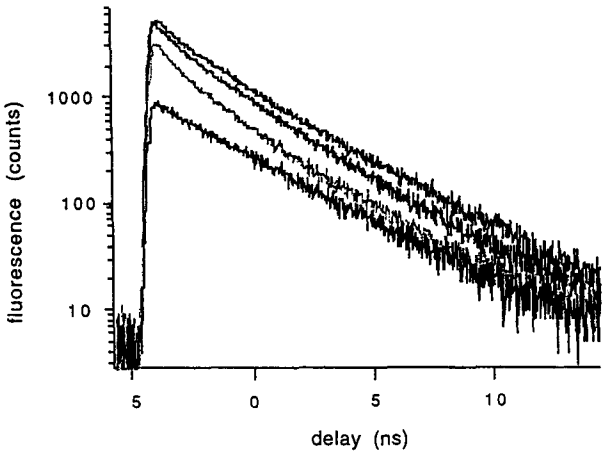

Fig. 14. Four decays recorded on pancreatic cells stained with calcium green. The decay curves obtained are different either because of a difference in the maturing level of cells or because of focusing on different organelles.

microscope optics. Both time-resolved fluorescence and anisotropy relaxations have been measured.

REFERENCES

1. R. P. Haugland (1996) *Handbook of Fluorescent Probes and Research Chemicals*, N.T.Z. Spence Ed. Molecular Probe Inc.
2. J. R. Lakowicz (1994) *Topics in Fluorescence Spectroscopy, Vol. 4. Probe Design and Chemical Sensing*, Plenum Press, New York and London.
3. M. Konishi *et al.* (1988) *Biophys. J.* **54**, 1089–1104.
4. R. Tsien and T. Pozzan (1989) *Methods in Enzymology, Vol. 172*, Academic Press, New York.
5. D. V. O'Connors and D. Phillips (1985) *Time Correlated Single Photon Counting*, Academic Press, London.
6. J.-P. Galaup, Laboratoire Aimé Cotton, 91405 Orsay Cedex, Université Paris Sud Orsay, France.
7. T. Wilson (Ed.) (1990) *Confocal Microscopy*, Academic Press, London.
8. H. Lami and E. Piémont (1992) *E. Chem. Phys.* **163**, 149–159.

9a. J. B. Pawley (1990) *Handbook of Biological Confocal Microscopy*, Plenum Press, New York and London.

9b. H. Qian and E. L. Elson (1991) *Appl. OPt.* **30**, No. 10.

10. E. L. Elson and D. Madge (1974) *Biopolymers* **13**, 1–27.
11. R. Rigler *et al.* (1993) *Eur. Biophys. J.* **22**, 169–175.
12. J. Mets and Ü. Rigler (1995) *J. Phys. Chem.* **99**, 13368–13379.
13. N. G. Van Kampen (1992) *Stochastic Processes in Physics and Chemistry* (Elsevier Science, Amsterdam).
14. H. Quian and E. L. Elson (1991) *Appl. Opt.* **30**, 1185–1195.
15. V. Veissier, J. L. Viovy, and L. Monnerey (1989) *J. Phys. Chem.* **93**, 1709–1713.
16. H. Masuhara, *Microphotoconversion Project*, Exploratory research for advanced technology program.

17a. Cantor, S. (1980) *Biophysical Chemistry, Part II*, Freeman, San Francisco.

17b. C. Kaowang, R. Liao, and H. C. Cheung (1992) *Biochim. Biophys. Acta* **1121**, 16–22.

18a. M. Vincent *et al.* (1992) *Eur. J. Biochem.* **210**, 953–961.

18b. G. R. Fleming (1986) *International Series of Monographs on Chemistry, 13. Chemical Applications of Ultrafast Spectroscopy*, Oxford Science, Oxford University Press, New York, Clarendon Press Oxford.

19. A. D. Stein *et al.* (1992) *J. Phys. Chem.* **96**, 5255–5263.
20. M. Konishi *et al.* (1988) *Biophys. J.* **54**, 1089–1104.
21. P. Pringsheim (1949) *Fluorescence et Phosphorescence*, Argonne Natinal Laboratory, Chicago, IL, Interscience, New York, pp. 370–379.
22. R. C. Weast (Ed.) (1983–1984) *Handbook of Chemistry and Physics*, 64th ed., CRC Press, Boca Raton, FL.